Bridging the waiting points: The role of two-proton capture reactions in the rp process

Joachim Görres and Michael Wiescher

University of Notre Dame, Department of Physics, Notre Dame, Indiana 46556

Friedrich-Karl Thielemann

Harvard-Smithsonian Center for Astrophysics, Cambridge, Massachusetts 02138
and Institut für Theoretische Physik, Universität Basel, CH-4056 Basel, Switzerland

The influence of two-proton capture reactions on long-lived waiting point isotopes near the proton drip line is discussed for the rp-process reaction flow. These reactions are characterized by two successive proton captures, where the first reaction product is unstable against proton emission, but the second reaction results in a particle stable nucleus. The reactions which have this character and involve long-lived waiting points in the rp process are $^{15}O(2p, \gamma)^{17}Ne$, $^{18}Ne(2p, \gamma)^{20}Mg$, and $^{38}Ca(2p, \gamma)^{40}Ti$. Their rates are presented and compared with the rates of alpha-induced reactions for stellar conditions at high temperatures and densities. We find that the two-proton captures on ^{15}O and ^{18}Ne can only compete for unrealistically high densities, but that $^{38}Ca(2p, \gamma)^{40}Ti$ can act as an efficient reaction link at conditions typical for x-ray bursts on neutron stars.

I. INTRODUCTION

The hot CNO cycles and the rp process have been proposed as the dominant nucleosynthesis processes in explosive hydrogen burning, which takes place most notably in cataclysmic binary systems, such as novae and x-ray bursts. At high temperature and density conditions in such environments the CNO cycles and the rp process are linked by the capture reaction sequence $^{15}O(\alpha, \gamma)^{19}Ne(p, \gamma)^{20}Na$, and the initial CNO material can be processed towards heavier nuclei as massive as Fe, Ni, and beyond. The nucleosynthesis time scale τ_{tot} depends on the sum of the individual reaction and decay times, τ_i,

$$\tau_{tot} = \sum_i \tau^i = \sum_i \left[\tau_\beta^i + (Y_p \rho N_A \langle \sigma v \rangle_{pi})^{-1} \right], \quad (1)$$

with Y_p indicating the hydrogen abundance and ρ the stellar density. The first term stands for a beta-decay time scale, the second term for the effective proton-capture time scale (see [1]). The main impedance for a continuous reaction flow between the CNO- and the FeNi-mass region are the waiting point nuclei ^{15}O ($T_{1/2}=122$ s), ^{18}Ne ($T_{1/2}=1.67$ s), and ^{38}Ca ($T_{1/2}=0.44$ s), as has been discussed in more detail by van Wormer *et al.* [1]. The compound nuclei ^{16}F, ^{19}Na, and ^{39}Sc formed by proton captures of these isotopes are particle unbound. This would imply that the processing of ^{15}O, ^{18}Ne, and ^{38}Ca to heavier nuclei has to wait for their β^+ decays. At high temperature and density conditions, however, these "waiting points" can be bridged by alpha-induced reactions and the rp process turns into the αp process [1,2].

In this work two-proton-capture reactions are discussed as an alternative for bridging these waiting point isotopes. They are similar in nature to the triple-alpha reaction, where ^8Be—produced by a first alpha reaction—is also unstable against alpha emission, and they are only possible because ^{17}Ne, ^{20}Mg, and ^{40}Ti are particle stable. Because of the short lifetimes of the product isotopes ($T_{1/2} \leq 0.1$ s), a fast two-proton-capture process could reduce the the nucleosynthesis time scale and increase the energy production rate in explosive hydrogen burning considerably.

In the following sections we will determine the reaction rates for such two-proton-capture reactions, adopting the two-step formalism described by Nomoto, Thielemann, and Miyaji [3]. We will calculate the reaction rates for $^{15}O(2p, \gamma)^{17}Ne$, $^{18}Ne(2p, \gamma)^{20}Mg$, and $^{38}Ca(2p, \gamma)^{40}Ti$ and compare them with the rates of β decays and α captures. This allows to determine temperature and density conditions at which extremely fast rp process nucleosynthesis and a high-energy generation may take place in hot hydrogen burning.

II. STELLAR REACTION RATES FOR TWO-PROTON-CAPTURE PROCESSES

Proton-capture reactions on ^{15}O, ^{18}Ne, and ^{38}Ca lead to an equilibrium between formation and breakup of the particle-unbound isotopes ^{16}F, ^{19}Na, and ^{39}Sc. The total production cross sections of ^{16}F, ^{19}Na, and ^{39}Sc are equal to the proton scattering cross sections of ^{15}O, ^{18}Ne, and ^{38}Ca, as proton emission is the only possible exit channel. For the purpose of generality let us denote the original target nucleus as 1, the product nucleus of the first capture as nucleus 2, and the product of the second capture as nucleus 3. The production rate for nucleus 2 is $\rho N_A \langle p, p \rangle_1 Y_p Y_1$. The decay is determined by

the decay width of nucleus 2, derived from $\Gamma\tau = \hbar$ or $\lambda_2 = 1/\tau_2 = \Gamma_2(E)/\hbar$. Thus, we have for the population of nucleus 2 the rate equation

$$\dot{Y}_2 = \rho N_A \langle p, p \rangle_1 Y_p Y_1 - \Gamma_2/\hbar Y_2. \tag{2}$$

Given that both processes are very fast if active at all, we have an equilibrium and $\dot{Y}_2 = 0$, i.e. $Y_2 = \rho N_A \langle p, p \rangle_1 (\hbar/\Gamma_2) Y_p Y_1$. In case we are interested in the population of nucleus 2 in a certain energy interval, we have

$$Y_2(E) = \rho N_A \left[\frac{d\langle p, p \rangle_1(E)}{dE} \right] \frac{\hbar}{\Gamma_2(E)} Y_p Y_1. \tag{3}$$

Here the differential denotes the integrand of the corresponding $\langle \sigma v \rangle$ integration. The energy dependence in the exit channel of the (p, p) reaction and $\Gamma_2(E)$ are identical and thus cancel out (for details see [3]). We can therefore replace $\Gamma_2(E)$ by $\Gamma_2 = \Gamma_2(E_r)$ at the resonance energy and treat in the (p, p) reaction only the incoming channel as energy dependent, while the exit channel is taken at the resonance energy, which changes Eq. (3) to

$$Y_2(E) = \rho N_A \left[\frac{d\langle p, p \rangle_1^*}{dE}(E) \right] \frac{\hbar}{\Gamma_2} Y_p Y_1. \tag{4}$$

A subsequent proton capture on nucleus 2 will lead to the production of the particle-stable isotopes ^{17}Ne, ^{20}Mg, and ^{40}Ti. The production of nucleus 3 via this second proton capture is described in the regular fashion. Its contribution from reactions passing through nucleus 2 at excitation energy E_2 is

$$\dot{Y}_3(E_2) = \rho N_A \left[\langle p, \gamma \rangle_2(E_2) \right] Y_p Y_2(E_2). \tag{5}$$

The rate of the second proton reaction and its Q value depend on the energy state of the target, i.e., nucleus 2. Therefore we use $\langle p, \gamma \rangle_2(E_2)$, and we have in general

$$\dot{Y}_3 = \rho^2 N_A^2 Y_p^2 Y_1 \frac{\hbar}{\Gamma_2} \int_0^\infty \left[\frac{d\langle p, p \rangle_1^*}{dE}(E_2) \right]$$
$$\times \left[\langle p, \gamma \rangle_2(E_2) \right] dE_2. \tag{6}$$

As such reaction sequences with an intermediate unstable nucleus are historically and formally described as three-body reactions, we have to correct for double counting of collisions between identical particles (here the two protons in the reaction). The three-body rate $\langle 1pp \rangle$ would be defined via $\dot{Y}_3 = (1/2)\rho^2 N_A^2 \langle 1pp \rangle Y_p^2 Y_1$. The so-defined two-proton capture rate can be expressed by equating this expression with Eq. (3), leading to

$$N_A^2 \langle 1pp \rangle = N_A^2 \frac{2\hbar}{\Gamma_2} \int_0^\infty \left[\frac{d\langle (p, p) \rangle_1^*}{dE}(E) \right]$$
$$\times \left[\langle (p, \gamma) \rangle_2(E) \right] dE. \tag{7}$$

If not only the unstable ground state of the intermediate nucleus 2 is involved, but also several excited resonance states, we can write in general

$$N_A^2 \langle 1pp \rangle = N_A^2 \sum_i \frac{2\hbar}{\Gamma_{2,i}} \int_0^\infty \left[\frac{d\langle (p, p) \rangle_{1,i}^*}{dE}(E) \right]$$
$$\times \left[\langle (p, \gamma) \rangle_{2,i}(E) \right] dE. \tag{8}$$

$\Gamma_{2,i}$ is the decay probability of the excited unbound compound nucleus state i, $d\langle (p, p) \rangle_{1,i}^*(E)/dE$ corresponds to its formation probability at energy E, and $\langle (p, \gamma) \rangle_{2,i}(E)$ is the reaction rate for the second proton capture with the target nucleus 2 in state i.

For the cases discussed here, the first proton capture populates the ground state and the first excited states of the particle unbound nuclei by resonant scattering. Also the second step can proceed via several resonances. In the terminology introduced by Fowler, Caughlan, and Zimmerman [4] the contribution of each of these resonances to the reaction rate $\langle \sigma v \rangle$ can be approximated by two analytical terms $\langle \sigma v \rangle_r$ and $\langle \sigma v \rangle_{nr}$, one corresponding to an approach where the resonance is approximated by a delta function (the so-called "resonant" contribution) and one which is dominated by the low-energy tail of the resonance, making use of a Breit-Wigner form of the resonance with the widths containing penetrabilities in the entrance and exit channels (the so-called "nonresonant" contribution). Below a certain temperature threshold, related to the resonance energy, the nonresonant term dominates, and above the temperature threshold the resonant term dominates. Below the corresponding temperature threshold of the first proton reaction nucleus 2 is produced in the low-energy tail of the resonance.

The resonance energies of the second proton capture reaction depend on the formation energy of nucleus 2. Above the temperature threshold of the first reaction the intermediate nucleus 2 is (predominantly) formed at the resonance energy. Therefore, the resonance energies of the second reaction become independent of the formation energy of nucleus 2 and the integral in Eq. (8) separates into two parts:

$$N_A^2 \langle 1pp \rangle = N_A^2 \sum_i \frac{2\hbar}{\Gamma_{2,i}} \langle (p, p) \rangle_{1,i}^* \langle (p, \gamma) \rangle_{2,i}. \tag{9}$$

Equations (8) and (9) differ in their results only for temperatures below the threshold of the first reaction (see Fig. 4 in [3]). Figures 1 and 2 result from performing the integral in Eq. (8) for the reactions ^{15}O$(2p, \gamma)^{17}$Ne and ^{18}Ne$(2p, \gamma)^{20}$Mg in exactly the same manner as the triple-alpha reaction was modeled by Nomoto, Thielemann, and Miyaji [3], making use of the dominant resonances listed in the tables of Appendix A. In each case the first two subsets show the reactions $\langle p, p \rangle_1$ and $\langle p, \gamma \rangle_2$ from (i) a numerical integration, (ii) the nonresonant analytical approach, and (iii) the resonant analytical approach. The temperature thresholds for the different target are ^{15}O $(3 \times 10^8$ K), ^{16}F $(1.3 \times 10^8$ K), ^{18}Ne $(9 \times 10^7$ K), ^{19}Na $(8 \times 10^8$ K), and (not shown here, also with resonance properties from tables in Appendix A) ^{38}Ca $(10^8$ K) and ^{39}Sc $(5 \times 10^7$ K), respectively. The third subset in each figure displays the total rate $N_A^2 \langle 1pp \rangle$ from (i) the general integral in Eq. (8), and (ii) the expression in Eq. (9), however, approximating $\langle p, p \rangle_1$ and $\langle p, \gamma \rangle_2$
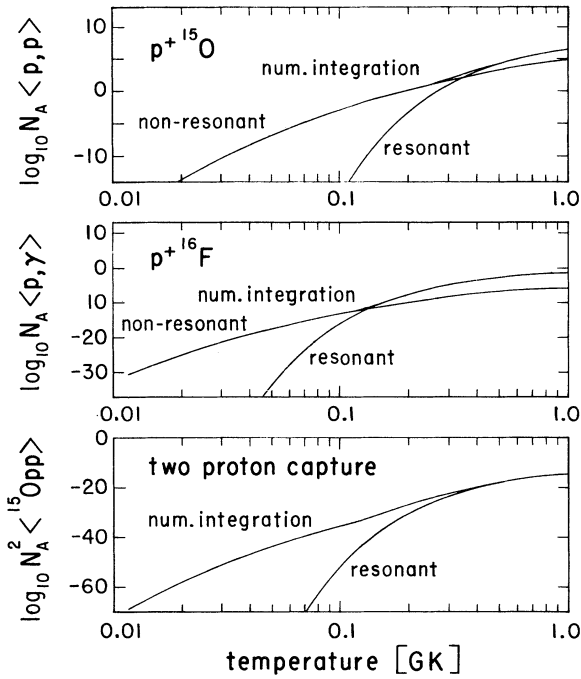
FIG. 1. The reaction rates for $^{15}O(p,p)$, $^{16}F(p,\gamma)^{17}Ne$, and the two-proton-capture reaction $^{15}O(2p,\gamma)^{17}Ne$ based on the dominant resonances listed in Appendix A. The calculations are performed as for the triple-alpha reaction by Nomoto, Thielemann, and Miyaji [3]. The first two subsets show the reaction $\langle p,p\rangle_1$ and $\langle p,\gamma\rangle_2$ from (i) a numerical integration, (ii) the nonresonant analytical approach, and (iii) the resonant analytical approach. The temperature thresholds beyond which the resonant rate dominates are 3×10^8 K for ^{15}O and 1.3×10^8 K for ^{16}F. The third subset displays the two-proton-capture reactions including the result from (i) a numerical integration and (ii) the purely resonant approximation without considering tail contributions. The temperature is measured in $T_9 = T/10^9$ K.
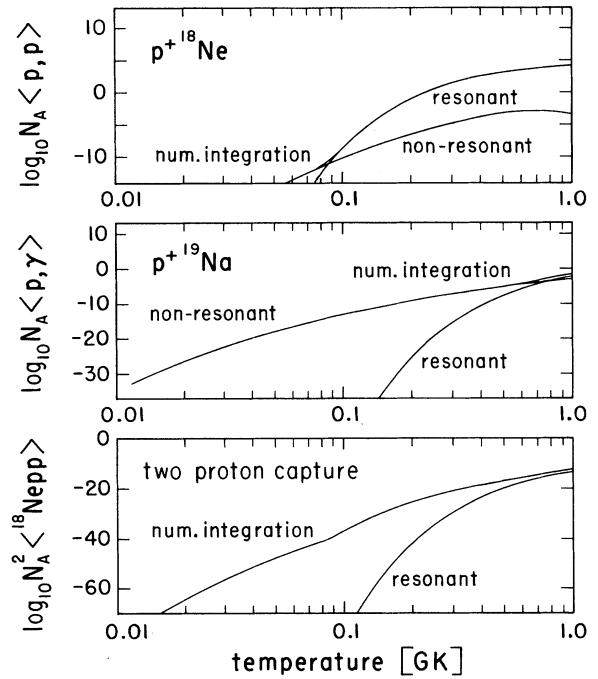
FIG. 2. The same as Fig. 1 for the reaction sequence $^{18}Ne(2p,\gamma)^{20}Mg$. The temperature thresholds for the validity of a purely resonant treatment are 9×10^7 K for ^{18}Ne and 8×10^8 K for ^{19}Na.

only by the resonant rate. We see that the purely resonant approach is not a good one and can be many orders of magnitudes off, but that the $2p$ captures on ^{15}O, ^{18}Ne, and ^{38}Ca can be calculated via the simpler equation (9) with the full expressions for the individual $\langle\sigma v\rangle$'s for temperatures beyond 3×10^8 K, 9×10^7 K, and 10^8 K, respectively. The latter two temperatures are smaller than

any typical rp-process conditions. Therefore we can use Eq. (9) for the targets ^{18}Ne and ^{38}Ca in any realistic application. The first reaction is a possible competitor with other breakout sequences from the hot CNO cycle (see [5]), which typically occur around 4×10^8 K. We will show in Sec. IV that the rate from Fig. 1 is not efficient enough to allow for any break-out from the hot CNO cycle via $^{15}O(2p,\gamma)^{17}Ne$ below temperatures of 3×10^8 K, and thus also this reaction can always be evaluated via Eq. (9) for our purposes.

III. RATE CALCULATIONS

The resonant rate for a resonance at energy E_i can be described in terms of the following analytical expression [4]:

TABLE I. Reaction rate for $^{15}O(p,p)^{15}O$, $^{16}F(p,\gamma)^{17}Ne$, and $^{15}O(2p,\gamma)^{17}Ne$.

T_9	$N_A\hbar\langle^{15}O(p,p)\rangle/\Gamma$		$N_A\langle^{16}F(p,\gamma)\rangle$		$N_A^2\langle^{15}O(2p,\gamma)\rangle$
	g.s.	First exc.	g.s.	First exc.	
0.3	1.7×10^{-19}	1.9×10^{-22}	8.6×10^{-5}	5.1×10^{-5}	2.9×10^{-23}
0.5	3.0×10^{-16}	7.1×10^{-18}	1.0×10^{-2}	1.4×10^{-3}	6.0×10^{-18}
0.6	1.8×10^{-15}	9.0×10^{-17}	3.2×10^{-2}	4.0×10^{-3}	1.2×10^{-16}
0.8	1.6×10^{-14}	1.2×10^{-15}	1.7×10^{-1}	2.0×10^{-2}	5.6×10^{-15}
1.0	5.3×10^{-14}	1.2×10^{-14}	4.5×10^{-1}	6.6×10^{-2}	5.0×10^{-14}
1.5	2.4×10^{-13}	1.1×10^{-13}	2.0	4.9×10^{-1}	1.1×10^{-12}
2.0	4.3×10^{-13}	2.9×10^{-13}	5.6	1.8	6.0×10^{-12}
3.0	6.5×10^{-13}	6.4×10^{-13}	2.3×10^1	9.5	4.3×10^{-11}
5.0	7.2×10^{-13}	9.2×10^{-13}	1.1×10^2	4.7×10^1	2.5×10^{-10}

TABLE II. Reaction rate for $^{18}\mathrm{Ne}(p,p)^{18}\mathrm{Ne}$, $^{19}\mathrm{Na}(p,\gamma)^{20}\mathrm{Mg}$, and $^{18}\mathrm{Ne}(2p,\gamma)^{20}\mathrm{Mg}$.

T_9	$N_A\hbar\langle^{18}\mathrm{Ne}(p,p)\rangle/\Gamma$			$N_A\langle^{19}\mathrm{Na}(p,\gamma)\rangle$			$N_A^2\langle^{18}\mathrm{Ne}(2p,\gamma)\rangle$
	g.s.	First exc.	Second exc.	g.s.	First exc.	Second exc.	
0.3	8.4×10^{-15}	5.5×10^{-17}	3.3×10^{-21}	2.5×10^{-7}	2.3×10^{-6}	1.3×10^{-6}	4.4×10^{-21}
0.5	5.5×10^{-13}	2.3×10^{-14}	5.1×10^{-17}	2.2×10^{-5}	2.1×10^{-4}	1.2×10^{-4}	3.3×10^{-17}
0.6	1.4×10^{-12}	9.7×10^{-14}	5.3×10^{-16}	9.5×10^{-5}	8.8×10^{-4}	5.0×10^{-4}	4.8×10^{-16}
0.8	4.4×10^{-12}	5.3×10^{-13}	8.9×10^{-15}	1.1×10^{-3}	7.9×10^{-3}	4.0×10^{-3}	1.8×10^{-14}
1.0	8.0×10^{-12}	1.4×10^{-12}	4.5×10^{-14}	7.9×10^{-3}	4.3×10^{-2}	1.6×10^{-2}	2.4×10^{-13}
1.5	1.5×10^{-11}	4.1×10^{-12}	3.3×10^{-13}	2.3×10^{-2}	7.6×10^{-1}	2.0×10^{-1}	6.8×10^{-12}
2.0	1.8×10^{-11}	6.2×10^{-12}	7.9×10^{-13}	1.4	3.7	8.7×10^{-1}	9.7×10^{-11}
3.0	1.8×10^{-11}	7.9×10^{-12}	1.6×10^{-12}	8.2	1.9×10^1	6.06	4.8×10^{-10}
5.0	1.4×10^{-11}	7.2×10^{-12}	2.1×10^{-12}	3.5×10^1	9.1×10^1	4.7×10^1	2.4×10^{-9}

$$\langle(p,p)\rangle_{1,i}^r = \left(\frac{2\pi}{\mu kT}\right)^{3/2}\hbar^2(\omega\gamma)_i\exp\left[-\frac{E_i}{kT}\right].\quad(10)$$

The resonance energies E_i are derived from the proton binding energies and the excitation energies of the particle unstable isotopes. The resonance strength $(\omega\gamma)_i$ is given by

$$(\omega\gamma)_i = \frac{2J_i+1}{2(2j_t+1)}\Gamma_{p,i}.\quad(11)$$

J_i and $\Gamma_{p,i}$ are the spins and the proton partial widths of the resonances, and j_t is the spin of the target nucleus. The proton partial widths are calculated as a function of the proton penetrability P_ℓ through the Coulomb and orbital momentum barrier and the single-particle spectroscopic factor C^2S of the resonant state

$$\Gamma_p = \frac{3\hbar}{\mu R^2}P_\ell C^2 S.\quad(12)$$

μ is the reduced mass, $R = 1.35(A_p^{1/3}+A_T^{1/3})$, and P_ℓ the Coulomb penetrability. The level parameters of the various compound nuclei are discussed and listed in Tables V–VII, and X in Appendix A. We discussed in Sec. II that the temperature region of astrophysical interest is beyond the threshold for the (p,p) reactions. Thus, we need only to consider the resonant rates of Eq. (10).

For each level i in the particle unstable nucleus the equilibrium abundance is determined by

$$\frac{Y_{2,i}}{Y_1} = \frac{\rho Y_p N_A\langle(p,p)\rangle_{1,i}\hbar}{\Gamma_{2,i}},\quad(13)$$

TABLE III. Reaction rate for $^{38}\mathrm{Ca}(p,p)^{38}\mathrm{Ca}$, $^{39}\mathrm{Sc}(p,\gamma)^{40}\mathrm{Ti}$, and $^{38}\mathrm{Ca}(2p,\gamma)^{40}\mathrm{Ti}$.

T_9	$N_A\hbar\langle^{38}\mathrm{Ca}(p,p)\rangle/\Gamma$	$N_A\langle^{39}\mathrm{Sc}(p,\gamma)\rangle$	$N_A^2\langle^{38}\mathrm{Ca}(2p,\gamma)\rangle$
	g.s.	g.s.	
0.3	2.2×10^{-20}	5.0×10^{-6}	2.1×10^{-25}
0.5	1.1×10^{-16}	4.7×10^{-4}	1.0×10^{-19}
0.6	8.9×10^{-16}	1.4×10^{-3}	2.4×10^{-18}
0.8	9.8×10^{-15}	5.5×10^{-3}	1.1×10^{-16}
1.0	4.1×10^{-14}	1.6×10^{-2}	1.3×10^{-15}
1.5	2.3×10^{-13}	1.5×10^{-1}	7.0×10^{-14}
2.0	4.6×10^{-13}	5.5×10^{-1}	5.2×10^{-13}
3.0	8.0×10^{-13}	1.9	3.0×10^{-12}
5.0	9.4×10^{-13}	4.3	8.0×10^{-12}

which is the integral of Eq. (4), written for each resonance. The secondary proton capture occurs for these equilibrium abundances of the excited states i. The reaction rate can be treated in terms of a radiative capture process with a resonant and a nonresonant contribution. The nonresonant part contains the one due to the tail of the resonance as discussed in Sec. II plus a direct capture contribution, which corresponds to resonance tails of low-lying bound states. For the resonant component of the reaction rate the resonance energies $E_{j,i}$ depend on the initial excitation energy E_i of the target nucleus 2:

$$E_{j,i} = E_j - (Q+E_i),\quad(14)$$

where the E_j's are the excitation energies in the final nucleus 3, and Q is the Q value for the second proton capture reaction. For the resonance strengths $\omega\gamma$ also the proton decay to the different excited states i in the target nucleus have to be taken into account:
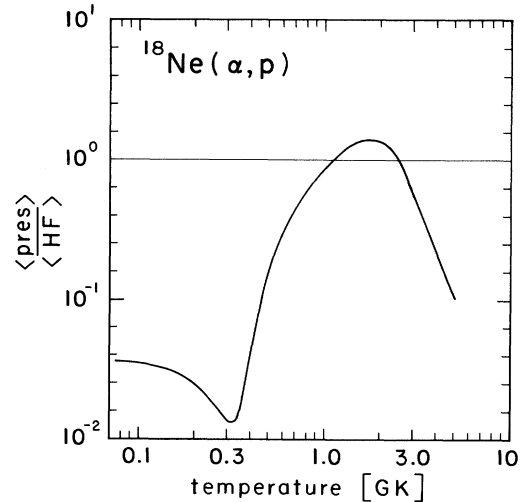

FIG. 3. Comparison of the predicted reaction rate for $^{18}\mathrm{Ne}(\alpha,p)^{21}\mathrm{Na}$, based on the level structure of the compound nucleus $^{22}\mathrm{Mg}$ and on Hauser-Feshbach calculations with the code SMOKER, respectively. For low temperatures the present rate is considerably lower than the Hauser-Feshbach prediction because of the low level density in $^{22}\mathrm{Mg}$. The disagreement at high temperatures is caused by the limited number of known levels at high excitation energies.

TABLE IV. Reaction rate for $^{18}\mathrm{Ne}(\alpha,p)^{21}\mathrm{Na}$, calculated from the level parameters of states in $^{22}\mathrm{Mg}$ and $^{22}\mathrm{Ne}$. Also shown are the Hauser-Feshbach rates, calculated with the code SMOKER, for $^{18}\mathrm{Ne}(\alpha,p)^{21}\mathrm{Na}$ and $^{38}\mathrm{Ca}(\alpha,p)^{41}\mathrm{Sc}$.

T_9	$N_A\hbar\langle^{18}\mathrm{Ne}(\alpha,p)\rangle_{(\mathrm{pres})}$	$N_A\langle^{18}\mathrm{Ne}(\alpha,p)\rangle_{(\mathrm{HF})}$	$N_A\langle^{38}\mathrm{Ca}(\alpha,p)\rangle_{(\mathrm{HF})}$
0.1	1.3×10^{-24}	4.4×10^{-25}	-
0.2	1.1×10^{-17}	4.5×10^{-16}	8.9×10^{-33}
0.3	1.0×10^{-13}	7.4×10^{-12}	8.8×10^{-26}
0.5	3.6×10^{-8}	2.4×10^{-7}	2.8×10^{-18}
0.8	4.2×10^{-4}	7.3×10^{-4}	4.9×10^{-14}
1.0	1.8×10^{-2}	2.1×10^{-2}	1.8×10^{-12}
1.5	7.2	4.0	4.8×10^{-10}
2.0	1.7×10^2	1.2×10^2	1.1×10^{-3}
3.0	3.4×10^3	6.4×10^3	9.6×10^{-1}
5.0	3.0×10^4	3.1×10^5	9.1×10^2

TABLE V. Resonance parameters for the $^{15}\mathrm{O}(p,p)^{15}\mathrm{O}$ reaction.

$E_x(^{16}\mathrm{F})$ (MeV)	$E_r^{\mathrm{c.m.}}$ (MeV)	J^π	C^2S	Γ_p (eV)[a]	$\omega\gamma$ (eV)
0.0	0.536	0^-	0.5	3.4×10^4	8.4×10^3
0.19	0.729	1^-	0.46	1.2×10^5	5.9×10^4
0.42	0.956	2^-	0.54	6.4×10^3	5.0×10^3

[a]For experimental values see Endt and van der Leun (1978).

TABLE VI. Resonance parameters for the $^{18}\mathrm{Ne}(p,p)^{18}\mathrm{Ne}$ reaction.

$E_x(^{19}\mathrm{Na})$ (MeV)	$E_x(^{19}\mathrm{O})$ (MeV)	$E_r^{\mathrm{c.m.}}$ (MeV)	J^π	C^2S	Γ_p (eV)	$\omega\gamma$ (eV)
0.0	0.0	0.320	$5/2^+$	0.57 [a]	1.1	3.4
0.12 [b]	0.096	0.440	$3/2^+$	0.01 [c]	0.27	0.54
1.35	1.472	0.673	$1/2^+$	1.00	4.6×10^4	4.6×10^4
2.96	3.067	3.278	$3/2^+$	0.06	4.8×10^4	9.6×10^4

[a]From $^{19}\mathrm{O}$, Ajzenberg-Selove (1983).
[b]Ajzenberg-Selove (1983).
[c]From $^{19}\mathrm{F}$, Ajzenberg-Selove (1983).

TABLE VII. Resonance parameters for the $^{38}\mathrm{Ca}(p,p)^{38}\mathrm{Ca}$ reaction.

$E_x(^{39}\mathrm{Sc})$ (MeV)	$E_x(^{39}\mathrm{Ar})$ (MeV)	$E_r^{\mathrm{c.m.}}$ (MeV)	J^π	C^2S	Γ_p (eV)	$\omega\gamma$ (eV)
0.0	0.0	0.599	$7/2^-$	0.62	3.4×10^{-3}	1.4×10^{-3}
0.95	1.267	1.549	$3/2^-$	0.5	6.7×10^3	1.3×10^4

TABLE VIII. Resonance parameters for the $^{16}\mathrm{F}(p,\gamma)^{17}\mathrm{Ne}$ reaction.

$E_x(^{17}\mathrm{Ne})$ (MeV)	$E_x(^{17}\mathrm{N})$ (MeV)	J^π	$E_{p_i}^{\mathrm{c.m.}}$ (MeV)	Γ_{p_i} (eV)[a]	Γ_γ (eV)	$\omega\gamma_i$ (eV)
1.850		$1/2^+$	0.359	1.9×10^2	1.6×10^{-5}	1.6×10^{-5}
			0.167	4.4×10^{-2}		1.1×10^{-9}
1.907		$5/2^-$	0.416	2.2×10^1	6.0×10^{-5}	1.8×10^{-4}
			0.224	2.5×10^{-2}		1.7×10^{-7}
2.526		$5/2^+$	1.036	1.9×10^2	2.0×10^{-5}	6.0×10^{-5}
			0.843	1.1×10^1		1.0×10^{-6}
3.204		$3/2^-$	1.714	5.6×10^3	2.2×10^{-2}	1.0×10^{-2}
			1.521	1.7×10^5		1.5×10^{-2}

[a]$C^2S_{\mathrm{g.s.}} = 0.5$, $C^2S_{1\mathrm{exc}} = 0.1$.

$$(\omega\gamma)_{j,i} = \frac{2J_j + 1}{2(2j_i + 1)} \frac{\Gamma_{p,j\to i}\Gamma_{\gamma,j}}{\Gamma_{\gamma,j} + \sum_n \Gamma_{p,j\to n}}. \quad (15)$$

The level parameters are also discussed in Appendix A. The resonant reaction rates are then given by

$$\langle(p,\gamma)\rangle_{2,i}^r = \left(\frac{2\pi}{\mu kT}\right)^{3/2} \hbar^2 \sum_j (\omega\gamma)_{j,i} \exp\left[-\frac{E_{j,i}}{kT}\right]. \quad (16)$$

In addition, the nonresonant contributions to the reaction rate have to be considered. This includes the tail contribution from the resonances and the low-lying bound states (the latter being referred to as direct capture). The tail contributions have been shown in Figs. 1

and 2 in the first two subsets. The S factor for the direct capture process can be calculated in a simple potential model [6] treating the process as a pure extra nuclear channel phenomenon while approximating the internal structure of the final state by scaling the theoretical S factor $S_{\mathrm{DC}}^{\mathrm{th}}$ with the single-particle spectroscopic factor $C^2 S_p$ of the final state, $S_{\mathrm{DC}} = C^2 S_p S_{\mathrm{DC}}^{\mathrm{th}}$. Included in the calculations is the direct capture transitions on the different excited levels i of the target nucleus to the final bound states j. The level parameters of the final states are also discussed in Appendix A.

Within the energy range considered here the S factor is essentially constant and the corresponding nonresonant reaction rate is described by

$$\langle(p,\gamma)\rangle_{2,i}^{\mathrm{nr}} = \left(\frac{2}{\mu}\right)^{1/2} \frac{\Delta}{(kT)^{3/2}} \sum_{i,j} S_{i\to j} \left(1 + \frac{5kT}{36E_0}\right) \exp\left[-\frac{3E_0}{kT}\right] \quad (17)$$

with Δ and E_0 as width and mean energy of the Gamow peak [7].

The total reaction rate for the secondary proton-capture process is given by the sum of the resonant and nonresonant contributions. We noticed that the tail contributions labeled in Figs. 1 and 2 as "nonresonant" are

much smaller than the direct capture terms. For this reason they were neglected.

The combined reaction rates for the two-proton-capture process has been calculated according to Eq. (9) and are listed in Tables I, II, and III as a function of temperature.
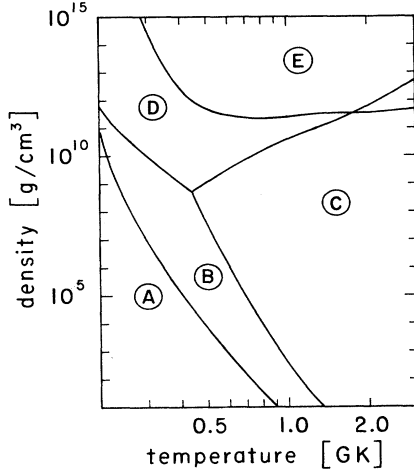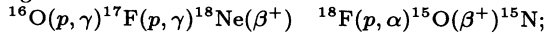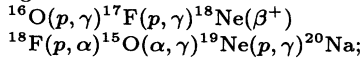

FIG. 4. Temperature and density conditions for two-proton capture as well as (α,p) reactions on ^{15}O and ^{18}Ne. The reaction flux in the different regions is characterized by one dominant reaction sequence.
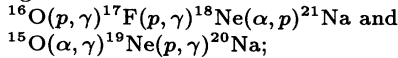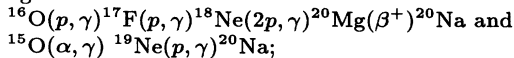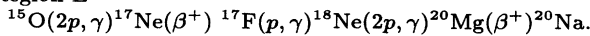
Region A
^{16}O$(p,\gamma)^{17}$F$(p,\gamma)^{18}$Ne(β^+) ^{18}F$(p,\alpha)^{15}$O$(\beta^+)^{15}$N;

Region B
^{16}O$(p,\gamma)^{17}$F$(p,\gamma)^{18}$Ne(β^+)
^{18}F$(p,\alpha)^{15}$O$(\alpha,\gamma)^{19}$Ne$(p,\gamma)^{20}$Na;

Region C
^{16}O$(p,\gamma)^{17}$F$(p,\gamma)^{18}$Ne$(\alpha,p)^{21}$Na and
^{15}O$(\alpha,\gamma)^{19}$Ne$(p,\gamma)^{20}$Na;

Region D
^{16}O$(p,\gamma)^{17}$F$(p,\gamma)^{18}$Ne$(2p,\gamma)^{20}$Mg$(\beta^+)^{20}$Na and
^{15}O(α,γ) ^{19}Ne$(p,\gamma)^{20}$Na;

Region E
^{15}O$(2p,\gamma)^{17}$Ne(β^+) ^{17}F$(p,\gamma)^{18}$Ne$(2p,\gamma)^{20}$Mg$(\beta^+)^{20}$Na.

IV. ASTROPHYSICAL IMPLICATIONS AND CONCLUSIONS

To evaluate the importance of the two-proton capture reactions for bridging the waiting point nuclei the rates have to be compared with the β-decay rates,
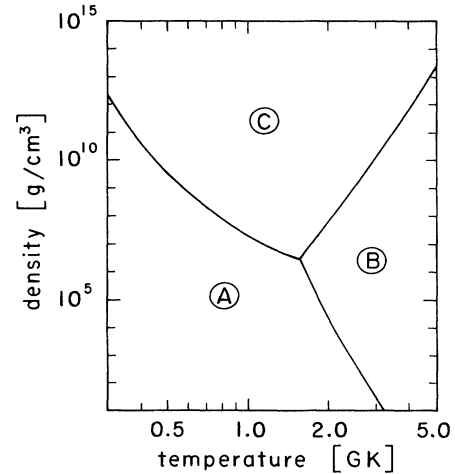
$$\lambda_\beta = \frac{\ln 2}{T_{1/2}}, \quad (18)$$

FIG. 5. Temperature and density conditions for a two-proton capture as well as an (α,p) reaction on ^{38}Ca. In region A, ^{38}Ca is mainly depleted via ^{38}Ca$(\beta^+)^{38}$K. In region B, via ^{38}Ca$(\alpha,p)^{41}$Sc and in region C, via ^{38}Ca$(2p,\gamma)^{40}$Ti.

TABLE IX. Direct capture (DC) parameters for the $^{16}F(p,\gamma)^{17}Ne$ reaction.

DC→ $E_f(^{17}Ne)$ (MeV)	l transfer	J^π	S factor (keV barn) [a]
DC→ 0.0	$s \to p$	$1/2^-$	0.33
DC→ 1.347	$s \to p$	$1/2^-$	0.34
DC* → 0.0	$s \to p$	$1/2^-$	0.12

[a]C^2S=0.1.

which are in first approximation temperature and density independent, and with the rates of the competing α-capture reactions on ^{15}O, ^{18}Ne, and ^{38}Ca. While the reaction rate for $^{15}O(\alpha,\gamma)^{19}Ne$ is theoretically and experimentally well studied [8,9], the reaction rate for $^{18}Ne(\alpha,p)^{21}Na$ is not known. The level density in the compound nucleus ^{22}Mg above the α threshold at 8.14 MeV is fairly high [10], however only natural parity states are populated in resonant α capture. Therefore, we estimated the rate from the known level structure of the mirror nucleus ^{22}Ne (see Appendix B). The resulting rate agrees fairly well with the predicted Hauser-Feshbach rate at the temperatures of interest, $T_9 \geq 0.6$, as shown in Fig. 3. The reaction rate of $^{38}Ca(\alpha,p)^{41}Sc$ is not known. The level density in the compound nucleus ^{42}Ti, however, is very high. Therefore, we also used a rate based on statistical model calculations with the code SMOKER (see the description in Sec. 3.4 of [11]). The rates are listed in Table IV as a function of temperature.

The comparison between the α-capture and the two-proton capture rates allows one to calculate the temperature and density conditions at which the two-proton capture dominate. Such stellar conditions would allow a fast depletion of ^{15}O and ^{18}Ne and fast leakage out of the hot CNO cycles towards higher masses. Figure 4 shows the temperature and density conditions at which different breakout reaction sequences will occur. The solid lines indicate the conditions at which competing $(2p,\gamma)$, (α,p), and (β^+)-decay rates are of equal strength. While the breakout via the α-capture reactions occurs at high temperatures the two-proton capture on ^{15}O and ^{18}Ne can only compete at extreme density conditions far above

$\rho = 10^9$ g/cm^3. This indicates that these two-proton capture reactions do not play a significant role for the fast breakout from the CNO cycles.

The situation, however, is different for the two-proton capture on ^{38}Ca, because the reaction rate for the competing (α,p) reaction is suppressed by a high Coulomb barrier. Therefore $^{38}Ca(2p,\gamma)$ allows a fast bridge from the mass range of sd-shell $(A \leq 40)$ to the mass range of fp-shell nuclei $(A \geq 40)$. Figure 5 demonstrates the temperature and density condition at which the two-proton-capture reaction is expected to dominate the reaction flow. The results indicate that $^{38}Ca(2p,\gamma)^{40}Ti$ can play a significant role at temperature and density conditions typical for x-ray burst scenarios [12,13]. Because the β decay of the waiting point nucleus ^{38}Ca is currently considered the main impedance for fast rp process nucleosynthesis at high temperatures and densities [1], bridging the β decay via $^{38}Ca(2p,\gamma)$ will reduce the nucleosynthesis time scale by a factor of 2.

APPENDIX A

1. The reaction rate of $^{15}O(p,p)$

The ground state of ^{16}F is proton unbound by $Q = -0.536$ MeV, therefore the ground state and the first two excited states in ^{16}F may be populated by elastic resonance scattering $^{15}O(p,p)^{15}O$. The excitation energies and the proton partial widths of these states are known [14]. The resulting resonance parameters are listed in Table V.

2. The reaction rate of $^{18}Ne(p,p)$

The ground state of ^{19}Na is proton unbound by $Q = -0.320$ MeV, therefore the ground state and several excited states in ^{19}Na may be populated by the

TABLE X. Resonance parameters for the $^{19}Na(p,\gamma)^{20}Mg$ reaction.

$E_x(^{20}Mg)$ (MeV)	$E_x(^{20}O)$ (MeV)	J^π	$E_{p_i}^{c.m.}$ (MeV)	Γ_{p_i} (eV)[a]	Γ_γ (eV)	$\omega\gamma_i$ (eV)
3.451	3.570	4^+	0.801	9.4×10^1	2.1×10^{-4}	1.2×10^{-4}
			0.681	3.2×10^1		6.0×10^{-5}
			0.448	2.5×10^{-4}		9.3×10^{-10}
3.857	4.072	2^+	1.207	4.1×10^4	8.9×10^{-2}	2.3×10^{-2}
			1.087	2.7×10^4		2.2×10^{-2}
			0.854	1.4×10^2		2.3×10^{-4}
4.317	4.456	0^+	1.667	5.6×10^3	1.4×10^{-3}	9.6×10^{-6}
			1.547	3.9×10^3		1.0×10^{-5}
			1.314	5.7×10^4		2.9×10^{-4}
4.699	4.850	4^+	2.049	1.4×10^4	2.6×10^{-3}	1.1×10^{-3}
			1.929	1.1×10^4		1.3×10^{-3}
			1.696	1.1×10^1		2.5×10^{-6}
4.978	5.234	2^+	2.328	2.9×10^5	2.9×10^{-1}	6.4×10^{-2}
			2.208	2.6×10^5		8.6×10^{-2}
			1.975	1.2×10^4		8.0×10^{-3}

[a]C^2S=0.1.

TABLE XI. Direct capture (DC) parameters for the ^{19}Na$(p,\gamma)^{20}$Mg reaction.

DC→ $E_f(^{20}$Mg) (MeV)	ℓ transfer	J^π	S factor (keV barn)[a]
DC→0.0	p → d	0$^+$	0.02
DC→1.547	p → s	2$^+$	1.11
DC* →0.0	p → d	0$^+$	0.03
DC* →1.547	p → s	2$^+$	1.65

[a]$C^2S=0.1$.

^{18}Ne$(p,p)^{18}$Ne reaction. Only the excitation energy of the first excited state in ^{19}Na is experimentally known [15], the energies of the higher excited states have been estimated from their Thomas-Ehrman shifts relative to their mirror levels in ^{19}O as described in [8]. The proton widths have been calculated using Eq. (4). The single-particle factors C^2S have been taken from shell-model calculations [16] if not listed otherwise. The resulting resonance parameters are listed in Table VI.

3. The reaction rate of ^{38}Ca(p,p)

The ground state of ^{39}Sc is proton unbound by $Q = -0.60$ MeV, the ground state and the first excited state will be populated in ^{38}Ca$(p,p)^{38}$Ca. The excitation energy of the first excited state is known [10], no information about the proton widths of the ground state and first excited state is available. The proton width has been calculated as described before, using the single-particle spectroscopic factors of the $T = 3/2$ mirror states in ^{39}K. The resulting resonance parameters are listed in Table VII.

4. The reaction rate of ^{16}F$(p,\gamma)^{17}$Ne

The stellar reaction rate of ^{16}F$(p,\gamma)^{17}$Ne has a positive Q value, $Q = 1.49$ MeV. The excited states in ^{17}Ne can be populated by resonant proton capture on the equilibrium abundances of the ground state and the first excited state in ^{16}F. Because the level parameters are not known, resonance energies and γ-decay widths have been adopted from the mirror states in ^{17}N. The proton partial widths have been calculated as described in Eq. (4), adopting a typical single-particle spectroscopic factor of $C^2S=0.1$. In all cases the proton partial widths are considerably larger than the γ partial widths. Therefore the proton partial widths cancel out and the resonance strengths are determined only by the γ partial widths of these levels. The final resonance parameters are listed in Table VIII.

The direct capture process is characterized by the

strong $s \rightarrow p$ transition from the ground state in ^{16}F (0^-) to the ground state $(1/2^-)$ and the first excited state at 1.347 MeV $(3/2^-)$ in ^{17}Ne. A smaller contribution results from the $s \rightarrow p$ direct capture on the first excited state in ^{16}F (1^-) to the ground state in ^{17}Ne. For the final states a single-particle spectroscopic factor of $C^2S=0.1$ has been adopted. The direct capture parameters are given in Table IX.

5. The reaction rate of ^{19}Na$(p,\gamma)^{20}$Mg

The Q value of the ^{19}Na(p,γ) reaction is $Q = 2.65$ MeV. Resonant capture, however, may occur not only on ^{19}Na in the ground state, but also in the first and second excited states. The energies of the proton unbound states in ^{20}Mg are not known and have therefore been derived from the known excitation energies in the mirror nucleus ^{20}O as described by [8]. There is also no information available about the proton and γ partial widths of the resonance levels. The proton widths have therefore been calculated as described above, adopting a "typical" single-particle spectroscopic factor of $C^2S=0.1$. The γ width has been calculated as single-particle decay strength for transitions to the ground state and the first excited state in ^{20}Mg, weighted with the mean of the Weisskopf strength distribution in this mass range [17]. The resulting resonance parameters are listed in Table X. For the nonresonant contribution we calculated the $p \rightarrow s,d$ direct capture to the ground state (0^+) and the first excited state in ^{20}Mg at 1.55 MeV (2^+), respectively. A spectroscopic factor of $C^2S=0.1$ has been adopted for both levels (see Table XI). While the resonances dominate the reaction rate at higher temperatures, $T_9 \geq 1$, the direct capture determines the lower temperature range.

6. The reaction rate of ^{39}Sc$(p,\gamma)^{40}$Ti

The reaction has a Q value of $Q = 2.18$ MeV. Because of the high excitation energy of the first excited state in ^{39}Sc only proton capture on the ground state of ^{39}Sc has been considered. No experimental information about the excited states in ^{40}Ti are available, excitation energies and γ partial widths have been adopted from the mirror states in ^{40}Ar [10]. The proton partial widths have been calculated as described before adopting a single-particle spectroscopic factor of $C^2S=0.1$. The resonance parameters are listed in Table XII.

The direct capture component in this reaction is characterized by a $d \rightarrow f$ wave transition to the ground state in ^{40}Ti. The S factor is very small, mainly due to the high Coulomb barrier and the direct capture contribution is negligible.

TABLE XII. Resonance parameters for the ^{39}Sc$(p,\gamma)^{40}$Ti reaction.

$E_x(^{40}$Ti) (MeV)	$E_x(^{40}$Ar) (MeV)	J^π	$E_{p_i}^{\text{c.m.}}$ (MeV)	Γ_{p_i} (eV)[a]	Γ_γ (eV)	$\omega\gamma_i$ (eV)
2.524	2.524	2$^+$	0.343	1.0×10^{-5}	2.0×10^{-3}	3.0×10^{-6}
2.892	2.892	4$^+$	0.711	4.3×10^{-1}	2.0×10^{-4}	1.0×10^{-4}
3.208	3.208	2$^+$	1.027	2.4×10^1	1.0×10^{-2}	3.0×10^{-3}

[a]$C^2S=0.1$.

TABLE XIII. Resonance parameters for the $^{18}\text{Ne}(\alpha,p)^{21}\text{Na}$ reaction.

$E_x(^{22}\text{Mg})$ (MeV)	$E_x(^{22}\text{Ne})$ (MeV)	J^π	$E_\alpha^{\text{c.m.}}$ (MeV)	S_α (eV)	$\omega\gamma$ (eV)
8.29	8.49	2^+	0.150	0.003	1.5×10^{-33}
	8.59	2^+	0.23	0.225	6.2×10^{-19}
8.55	8.74	3^-	0.41	0.012	7.8×10^{-13}
	8.98	4^+	0.65	0.06	3.9×10^{-8}
	9.10	3^-	0.96	0.05	8.4×10^{-4}
	9.72	3^-	1.58	0.08	4.0
	9.84	2^+	1.70	0.09	4.6×10^1
	10.05	0^+	1.91	0.4	9.8×10^2

APPENDIX B

1. The reaction rate of $^{18}\text{Ne}(\alpha,p)^{21}\text{Na}$

The resonant α capture on ^{18}Ne populates the compound nucleus ^{22}Mg at high excitation energies, $E_x \geq 8.14$ MeV. Despite the high level density in ^{22}Mg at this excitation range the selection rules for the resonant α capture on a $J^\pi = 0^+$, $T = 1$ nucleus allow only to populate natural parity, $T = 1$ compound levels in ^{22}Mg. This may reduce the effective level density significantly. A statistical Hauser-Feshbach treatment for the reaction rate seems therefore questionable.

The reaction rate for $^{18}\text{Ne}(\alpha,p)^{21}\text{Na}$ was calculated from the resonance strengths of the α-unbound natural parity states in ^{22}Mg. While only two such states are known in ^{22}Mg itself, $E_x = 8.29$ MeV and 8.55 MeV [10], the mirror nucleus ^{22}Ne shows a considerable number of natural parity states in this excitation range. Table XIII lists the experimentally known excitation energies. The here suggested analog assignment is based on the observed transition strengths in the mirror two-particle transfer reactions $^{20}\text{Ne}(^3\text{H},p)^{22}\text{Ne}$ [18] and $^{20}\text{Ne}(^3\text{He},n)^{22}\text{Mg}$ [19], which also populate selec-

tively natural parity states. The resonance energies for $^{18}\text{Ne}(\alpha,p)$ have been estimated, taking into account an averaged level shift of 0.194 MeV. The spin and parities for the levels are based on recent $^{18}\text{O}(^6\text{Li},d)^{22}\text{Ne}$ angular distribution measurements [20]. The resonance strength for the different levels,

$$\omega\gamma = (2J + 1)\frac{\Gamma_\alpha\Gamma_p}{\Gamma_{\text{tot}}} \qquad (\text{B1})$$

depends mainly on the small α partial widths, $\Gamma_\alpha \ll \Gamma_p \approx \Gamma_{\text{tot}}$. The α partial widths are calculated as described before, the α spectroscopic factors result from the $^{18}\text{O}(^6\text{Li},d)^{22}\text{Ne}$ α-transfer studies to the mirror states [20]. The resonance parameters are also listed in Table XIII. Table IV compares the reaction rate calculated from the resonance parameters with the Hauser-Feshbach rate calculated with the code SMOKER [11]. In the low-temperature region $T_9 \leq 0.5$ the resonant rate is significantly smaller than the Hauser-Feshbach rate, good agreement however is observed in the temperature range between $T_9 = 1$ and $T_9 = 3$. The disagreement at higher temperatures is explained by the limited number of known levels at higher excitation energies included in the calculation.

[1] L. Van Wormer, J. Görres, C. Iliadis, M. Wiescher, and F.-K. Thielemann, Astrophys. J. **432**, 236 (1994).

[2] R.K. Wallace and S.E. Woosley, Astrophys. J. **45**, 389 (1981).

[3] K. Nomoto, F.-K. Thielemann, and S. Miyaji, Astron. Astrophys. **149**, 239 (1985).

[4] W.A. Fowler, G.R. Caughlan, and B.A. Zimmerman, Annu. Rev. Astron. Astrophys. **5**, 525 (1967).

[5] M. Wiescher, V. Harms, J. Görres, F.-K. Thielemann, and L. Rybarcyk, Astrophys. J. **316**, 162 (1987).

[6] C. Rolfs, Nucl. Phys. **A217**, 29 (1973).

[7] C.E. Rolfs and W.S. Rodney, *Cauldrons in the Cosmos* (University of Chicago Press, Chicago, 1988).

[8] K.H. Langanke, M. Wiescher, W.A. Fowler, and J. Görres, Astrophys. J. **301**, 629 (1986).

[9] P.V. Magnus, M.S. Smith, A.J. Howard, P.D. Parker, and A.E. Champagne, Nucl. Phys. **A506**, 332 (1990).

[10] P.M. Endt, Nucl. Phys. **A521**, 1 (1990).

[11] J.J. Cowan, F.-K. Thielemann, and J.W. Truran, Phys. Rep. **208**, 268 (1991).

[12] R.E. Taam, Annu. Rev. Nucl. Sci. **35**, 1 (1985).

[13] W.H.G. Lewin, J. van Paradijs, and R.E. Taam, Space Sci. Rev. **62**, 223 (1993).

[14] F. Ajzenberg-Selove, Nucl. Phys. **A460**, 1 (1986).

[15] F. Ajzenberg-Selove, Nucl. Phys. **A475**, 1 (1987).

[16] E.C. Halbert, J.B. McGrory, B.H. Wildenthal, and S.P. Pandya, in *Advances in Nuclear Physics*, edited by M. Baranger and E. Vogt (Plenum Press, New York, 1971), Vol. 4, p. 316.

[17] P.M. Endt, At. Data Nucl. Data Tables **23**, 3 (1979).

[18] E.R. Flynn, O. Hansen, and O. Nathan, Nucl. Phys. **A228**, 189 (1974).

[19] W.P. Alford, P. Craig, D.A. Lind, R.S. Raymond, J. Ullman, C.D. Zafiratos, and B.H. Wildenthal, Nucl. Phys. **A457**, 317 (1986).

[20] U. Giesen, C.P. Browne, J. Görres, S. Graff, C. Iliadis, H.P. Trautvetter, M. Wiescher, V. Harms, K.L. Kratz, B. Pfeiffer, R.E. Azuma, M. Buckby, and J.D. King, Nucl. Phys. **A561**, 95 (1993).